Check for updates

Received: 13 February 2023 | Accepted: 24 May 2023

DOI: 10.1002/nsg.12261

Near Surface Geophysics EAGE EUROPEAN ASSOCIATION OF GEOSCIENTISTS & ENGINEERS

ORIGINAL ARTICLE

A joint geophysical approach to tune an integrated sinkhole monitoring method in evaporitic environments

Chiara Calligaris | **Emanuele Forte** | **Alice Busetti** | **Luca Zini**

Department of Mathematics and Geosciences, University of Trieste, Trieste, Italy

Correspondence
Alice Busetti, Department of Mathematics and Geosciences, University of Trieste, Trieste 34128, Italy.
Email: abusetti@units.it

Funding information
Regione Autonoma Friuli Venezia Giulia; Realizzazione del censimentoregionale dei sinkhole e relativo GIS con corso formativo e predisposizionedelle linee guida di rilevamento ed informatizzazione nonché glossario deitermini utilizzati, Grant/Award Number: CUP: J92F16001310002; Accordo attuativo di collaborazione per la definizione e quantificazionedella pericolosità dei sinkhole nei litotipi evaporitici Permiani; Accordo attuativo di collaborazione per lamisurazione delle geometrie e delle deformazioni indotte dalla presenza disinkhole; Accordo attuativo dicollaborazione per l'aggiornamento censimento e pericolosità dei sinkhole delterritorio regionale

Abstract

Several methodologies allow for the detection and mapping of existing sinkholes in order to asses and manage the associated hazards and risks. These phenomena, linked to the presence of soluble rocks, are well known globally as they can cause severe damage to man-made structures. In this paper, we propose an integrated method applied to a test-site area in NE Italy where, on May 11 2017, a failure shaped like a sinkhole, suddenly occurred along a main regional road, which then had to be closed to traffic in part as a result of a landslide developing on the slope just upstream from the surface depression which had already formed. The slope was reprofiled, a paved barrier was placed at the toe of the slope, and the road itself was finally repaired and restored. In the test site, a detailed morphological and geological survey was performed, as well as several integrated multi-scale geophysical investigations, both in correspondence to the sinkhole location and in surrounding areas where other depressions were found. Results confirm the absence of large cavities down to the maximum investigated depth and highlighted a complex geological situation with abrupt lateral variations, a straight correlation between different geomorphological and geological elements, and the role of water paths. Geophysical investigations were found to be a useful tool to monitor the future evolution of the identified phenomena and to prevent further collapses and disasters along roads.

KEYWORDS
electrical resistivity tomography, geohazard, ground-penetrating radar, hydrogeology, sinkhole

INTRODUCTION

Sinkholes, that are natural sub-circular depressions of various dimensions and depths, are caused by the dissolution of soluble rocks or deposits in addition to internal erosion and/or gravitational processes (Gutiérrez, 2016; Parise, 2015; Waltham et al., 2005). These phenomena are globally widespread, for example in France (Thierry et al., 2009), Germany (Dahm et al., 2010; Krawczyk et al., 2012) Lithuania (Paukstys et al., 1999), Russia (Koutepov et al., 2008), Spain (Gutiérrez et al., 2008; Sevil et al., 2020), the United Kingdom (Cooper, 1998; Cooper et al., 2011), Albania (Parise et al., 2004), USA (Kuniansky et al., 2016), South Africa (Buttrick & van Schalkwyk, 1998), Iran (Karimi & Taheri, 2010; Taheri et al., 2015, 2019) and Italy (Busetti et al., 2020; Calligaris et al., 2017a, 2020; De Waele et al., 2017; Nisio, 2008 and all the references therein). They often have serious consequences in urban areas, causing physical and socio-economic damage to existing man-made structures and have a high risk factor due to their rapid occurrence and evolution (Intrieri et al., 2015; Martinotti et al., 2017; Zini et al., 2015 and all the references therein). Unfortunately, it is nearly impossible to precisely predict when and where sinkholes will occur, while monitoring the evolution of those which have already developed is somehow easier (Calligaris et al., 2019; Galve et al., 2011; Parise, 2015). Studying these

This is an open access article under the terms of the Creative Commons Attribution-NonCommercial-NoDerivs License, which permits use and distribution in any medium, provided the original work is properly cited, the use is non-commercial and no modifications or adaptations are made.
© 2023 The Authors. *Near Surface Geophysics* published by John Wiley & Sons Ltd on behalf of European Association of Geoscientists and Engineers.

geo-hydrological hazards more in-depth would facilitate a better understanding of their prodromal and triggering factors in order to prevent their intrinsic hazard and risk.

The implementation of sinkhole inventories (Calligaris et al., 2017b; Gutiérrez, 2016) is the first essential step in the evaluation of sinkhole hazard and risk assessment and is used as the basis to forecast the spatial and temporal distribution of future phenomena. In other words, the presence of old sinkholes is the best predictor for the potential occurrence of new ones. In addition, once inventoried, it is necessary to find a method to predict new phenomena in order to avoid serious accidents, specifically in urban areas or along the main roads and infrastructures. Different surface and subsurface investigation methods to identify and characterize sinkholes have been applied throughout the world. Among the others, we can report aerial and satellite image analysis (Dou et al., 2015; Festa et al., 2012; Gutiérrez et al., 2011; Panno & Luman, 2013), topographic map analysis (Basso et al., 2013; Brinkmann et al., 2008; Gutiérrez et al., 2011), field surveys (Bruno et al., 2008; Gutiérrez et al., 2007), LiDAR (Kim et al., 2019; Zhu et al., 2014, 2020), InSAR (Baer et al., 2018; Busetti et al., 2020; Galve et al., 2015; Guerrero et al., 2021; Intrieri et al., 2015; Jones & Blom, 2014; Malinowska et al., 2019; Oliver-Cabrera et al., 2020; Orhan et al., 2021; Shi et al., 2019; Solari et al., 2020; Theron et al., 2017), ground-based monitoring (Desir et al., 2018; Kersten et al., 2017; Kobe et al., 2019; Sevil et al., 2017; Zhende et al., 2013), geophysical surveys (De Ritis et al., 2020; García-Moreno & Mateos, 2011; Krawczyk et al., 2012; Kühn et al., 2011; Margiotta et al., 2012; Malehmir et al., 2016; Pazzi et al., 2018; Ronen et al., 2019; Samyn et al., 2014; Stierman, 2004; Waltham et al., 2005; Wust-Bloch & Joswig, 2006), hydrogeochemical studies (Delkhahi et al., 2020; Taheri et al., 2021) and trenching (Carbonel et al., 2015; Gutiérrez et al., 2018; Sevil et al., 2017) have been used in a series of multidisciplinary and multi-technique investigations.

In correspondence of residential zones or along the roads, limited-dimension sinkholes are immediately filled in order to restore infrastructures and reuse the territory. However, filling the sinkhole with coarse material does not eliminate its cause, but at worst can make the situation more dire due to the additional loading. This situation is particularly dangerous when infrastructures are built-up above a sinkhole area, which, due to their construction methods and the materials used (asphalt, reinforced concrete, etc), have a high resistance to breakage and can therefore favour the creation over time of even large voids immediately below the structures themselves, which eventually instantaneously collapse with serious risk to human safety (Pearson, 2013).

In Italy and, in particular, in the Friuli Venezia Giulia region (FVG), NE Italy, some of the mountain municipalities are characterized by the presence of evaporite bedrock and are heavily affected by sinkholes with serious consequences for infrastructures (Calligaris et al., 2017a, 2020). On May 11, 2017, in Baus, a hamlet situated North of the village of Ovaro (Figure 1), a subsidence phenomenon, suddenly occurred affecting regional road n. 355, one of the main N–S connections in the area, which then had to be closed to traffic. No one was crossing the road when the collapse occurred and subsequent vehicles were able to stop in time, thus avoiding a disaster. Due to the importance of the regional road with heavy traffic, the depression which had formed was immediately filled in with incoherent material, creating a concrete foundation and restoring the asphalt.

Several integrated multi-scale geophysical investigations, including electrical resistivity tomography (ERT), refraction seismic (RS), Ground Penetrating Radar (GPR) and electromagnetic induction (frequency domain electromagnetic [FDEM]), were performed on the road at the location of the sinkhole and in surrounding areas where other depressions were found in order to better understand the phenomena which had occurred, the triggering causes, the geological background and to monitor the state of activity and evolution over time. The novelty of the study is not only related to the use of combined electrical, seismic and multi-frequency electromagnetic techniques but also to their link with geological and geomorphological evidence. This integrated multi-scale geophysical approach allows for the non-invasive investigation and characterization of the subsurface as comprehensively as possible.

STUDY AREA

The hamlet of Baus is situated on the left alluvial terrace of the Degano Torrent and, according to Venturini et al. (2009), is built-up on a Permian evaporite and carbonate bedrock of the Bellerophon Fm. (BEL1 and BEL2). The evaporites are predominantly white and saccharoidal gypsum thinly interbedded with grey marls. The carbonates are dolostones and brown and grey limestones often in the form of cohesive granular rock. The Bellerophon Fm., which is in direct stratigraphic overlap with the Werfen Fm. (WER), does not outcrop extensively in the valley floor and it is mainly mantled by quaternary moraine deposits, Pleistocene in age and alluvial deposits, Holocene in age (Figure 1). Among the tectonic features, a regional structural discontinuity called the Sauris Thrust, approximately E–W oriented, crosses the study area to the South. It is included in those deformation structures, characterizing the FVG region, with low dipping angles that determined the

18730604, 2023, 5, Downloaded from https://onlinelibrary.wiley.com/doi/10.1002/nsg.12261 by Universita Di Trieste, Wiley Online Library on [28/01/2025]. See the Terms and Conditions (https://onlinelibrary.wiley.com/terms-and-conditions) on Wiley Online Library for rules of use; OA articles are governed by the applicable Creative Commons License

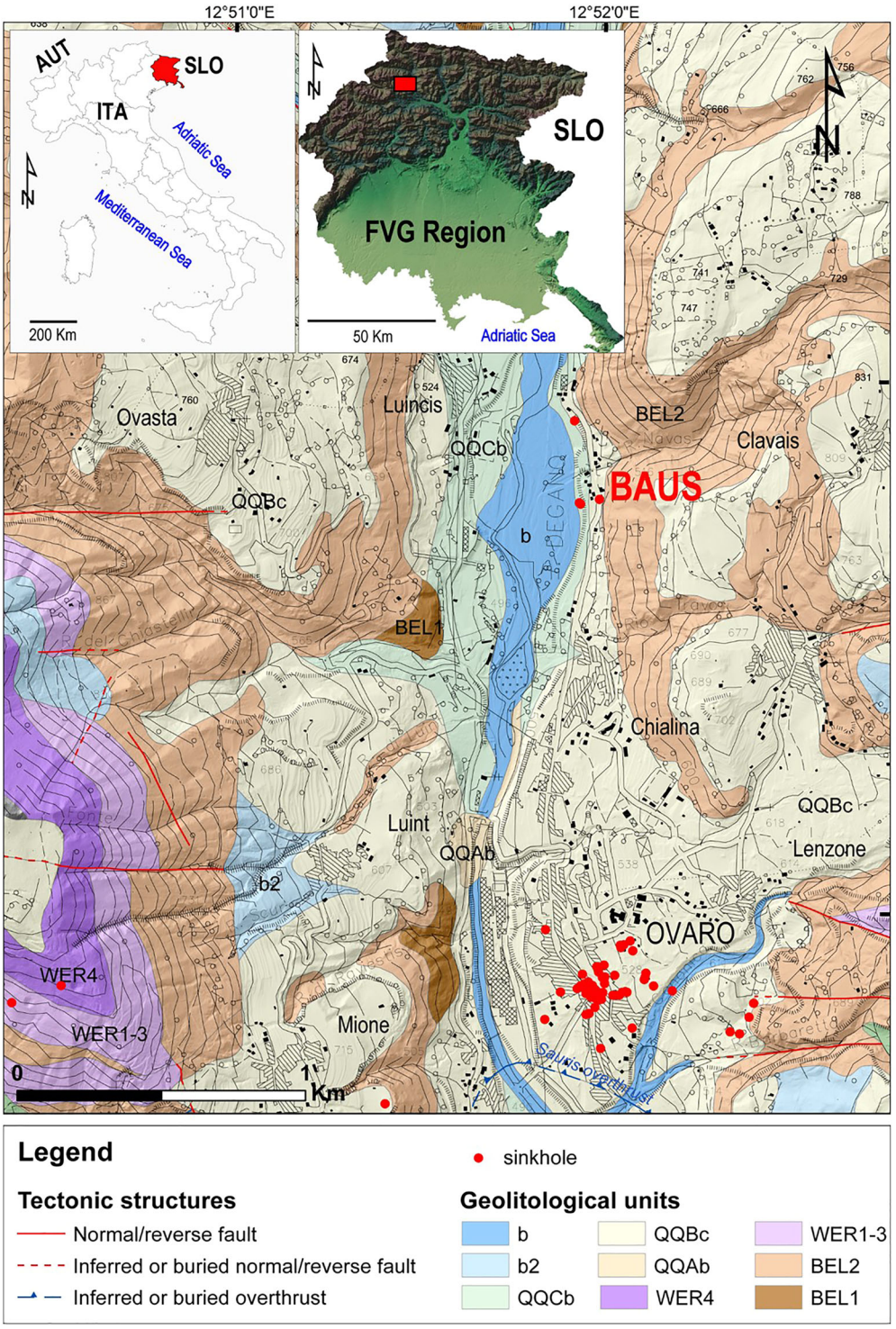

FIGURE 1 Geological map of the study area. Lithological quaternary units: (b) recent alluvial deposits; (b2) eluvial–colluvial deposits; (QQCb) gravels and fluvial sands; (QQBc) diamicton and till; (QQAb) fluvial and delta conglomerates. Permian–Triassic lithological units: Werfen Formation with (WER 4) laminated calcisyltites of the Siusi Member and (WER1-3) oolithic and micritic algal limestone, grey limestone and dolomites and dolomitic limestone; Bellerophon Formation with the dolomites and black limestone Member (BEL2) and gypsum and black dolomites Member (BEL1) (Venturini et al., 2009 – Foglio 31 Ampezzo).

superimposition of the Upper Permian sequences and Lower-Medium Triassic on Carnian units.

From a geomorphological point of view, the municipality of Ovaro is characterized by different elements; reliefs reaching 2075 m a.s.l. (Mt. Col Gentile) are separated by E–W valleys, which join the N–S oriented Degano River Valley. Notable terraces typify the valley floor which experienced different erosional and alluvial phases after the flow reversion of the Degano Torrent, which occurred in the post Last Glacial Maximum as suggested by

18730604, 2023, 5, Downloaded from https://onlinelibrary.wiley.com/doi/10.1002/nsg.12261 by Universita Di Trieste, Wiley Online Library on [28/01/2025]. See the Terms and Conditions (https://onlinelibrary.wiley.com/terms-and-conditions) on Wiley Online Library for rules of use; OA articles are governed by the applicable Creative Commons License

Venturini et al. (2009). The alluvial terrace deposits partially mantle the moraines abandoned during the retreat of the glacier tongue. These types of deposits can also be identified on the mountain slopes and highlands.

One of the geomorphological features characterizing the municipality of Ovaro are the sinkholes; phenomena associated with an iperkarst linked to the presence of the evaporites in the subsurface. The 93 sinkholes identified in the area were classified according to Gutiérrez et al. (2014) as follows: 11 bedrock collapses; 9 caprock collapses; 16 cover collapses; and 7 cover suffosion sinkholes. The remaining 50 do not have a precise typological attribution due to a lack of information, most being recognized in 1997 using mainly low-resolution vintage geophysical data (Cucchi & Giorgetti, 1997) and being at present no longer identifiable in the field, thus preventing a typological attribution. The diameters of the inventoried phenomena are very different, bedrock collapse sinkholes are in the range between 2 × 2 m and 49 × 67 m, caprock collapse sinkholes range between 36 × 38 m and 85 × 104 m, cover collapse sinkholes between 1 × 1 m and 30 × 34 m whereas cover suffosion between 1 × 1 m and 2 × 4 m. Considering the depths, in the whole data set they range between 0.5 m and 30 m. Excluding the undefined type, 38.5% are circular, 38.5% sub-circular, 17% elliptical, and 6% have an irregular shape. Overall, 40% are classified as active, 38% as dormant, 20% inactive, and 2% are artificially stabilized. Among the active phenomena, in 2014 and at the end of October 2018, two reactivations of previously known events located in the centre of the village of Ovaro, very close to some houses, bore witness to a quickly evolving situation (Calligaris et al., 2017a; Pearson, 2013).

In the hamlet of Baus, the study area of the present research, three sinkholes which developed on the alluvial terraces of the Degano Torrent have been identified: one is located in a flat zone on the N of Baus (Figure 2a,b); the other two are downstream from regional road 355, at almost the same elevation as the actual torrent bed (Figure 2c,d). The latter two were initially separated, but they are currently almost coalescent into an approximately 6 × 6 m single depression (Figure 2d).

In the proximity to the area where the above-mentioned sinkholes are present, on May 11 2017, along regional road n. 355 in the Degano Valley, a failure shaped like a sinkhole occurred (Caproni, 2017). The road, which is one of the main N–S connections among the mountain valleys in the Carnian Alps, had to be closed to the traffic which prevented people from moving freely and caused notable economic loss.

The event (about 14 m × 5 m) was elliptical in shape with the major axis parallel to the road. The maximum relative deepening was equal to 55 cm (Figure 2e). At the time of the event, the surveys highlighted three different alignments of traction cracks along the slope above the road (Figure 3, in orange). Recently (December 7, 2021), a new traction crack was identified at an altitude of 532 m a.s.l. (i.e., 21 m above the roadway), in the middle of the slope. It has a length of about 20 m and an average opening of about 20 cm with a depth of about 1.5 m (Figure 3, in purple).

After the event, the road was immediately repaired in order to guarantee it was both functional and safe. Important mitigation works were done reprofiling the slope and placing a paved barrier at its toe (Figure 2f).

MATERIALS AND METHODS

After the event occurred, seven crack-metres (CM) were installed on the existing infrastructures and buildings in order to monitor the area and define the state of activity of the movement. To define the depth of the bedrock and to monitor the ongoing situation, geophysical multi-scale integrated investigations were carried out in two different periods, namely on February 13, 2020, N of Baus in correspondence with the sinkhole pictured in Figure 2a, across the depression (Profile 3 – Figure 3) and downstream from the main event (Profile 2 – Figure 3) and on March 26, 2021, along regional road n. 355, in correspondence with the sinking phenomena which occurred in 2017 (Profile 1 – Figure 3).

Table 1 reports some details about the geophysical methods applied and the instruments used, whereas Table 2 lists the software and algorithms applied for data analysis, processing, and inversion for the various techniques exploited and their main parameters.

We decided to use an integrated and multi-scale approach to characterize not only the area along the road in which the sinkhole developed, but also in correspondence with two other zones where other previously unknown sinkhole phenomena were detected during the geomorphological field survey. In particular, we combined ERT with RS to infer the geological setting in the first 20–30 m below the surface, also evaluating possible lateral variations, whereas we integrated GPR with FDEM to characterize the first 4–5 m in the area of the former sinkhole along the road.

All the data sets were at first separately processed and analysed, and then integrated to obtain a more constrained and 'self-validated' interpretation. Such a multi-scale approach was made possible by the accurate positioning of all the collected data and sensors geometry measured with an RTK GPS device having centimetric accuracy.

Before ERT, RS and FDEM data inversion, a careful data quality check was performed in order to highlight and remove outliers or data having low statistical consistence. In particular, we compared ERT data collected with Wenner and Wenner–Schlumberger electrode configurations along the same path considering

18730604, 2023, 5, Downloaded from https://onlinelibrary.wiley.com/doi/10.1002/nsg.12261 by Universita Di Trieste, Wiley Online Library on [28/01/2025]. See the Terms and Conditions (https://onlinelibrary.wiley.com/terms-and-conditions) on Wiley Online Library for rules of use; OA articles are governed by the applicable Creative Commons License

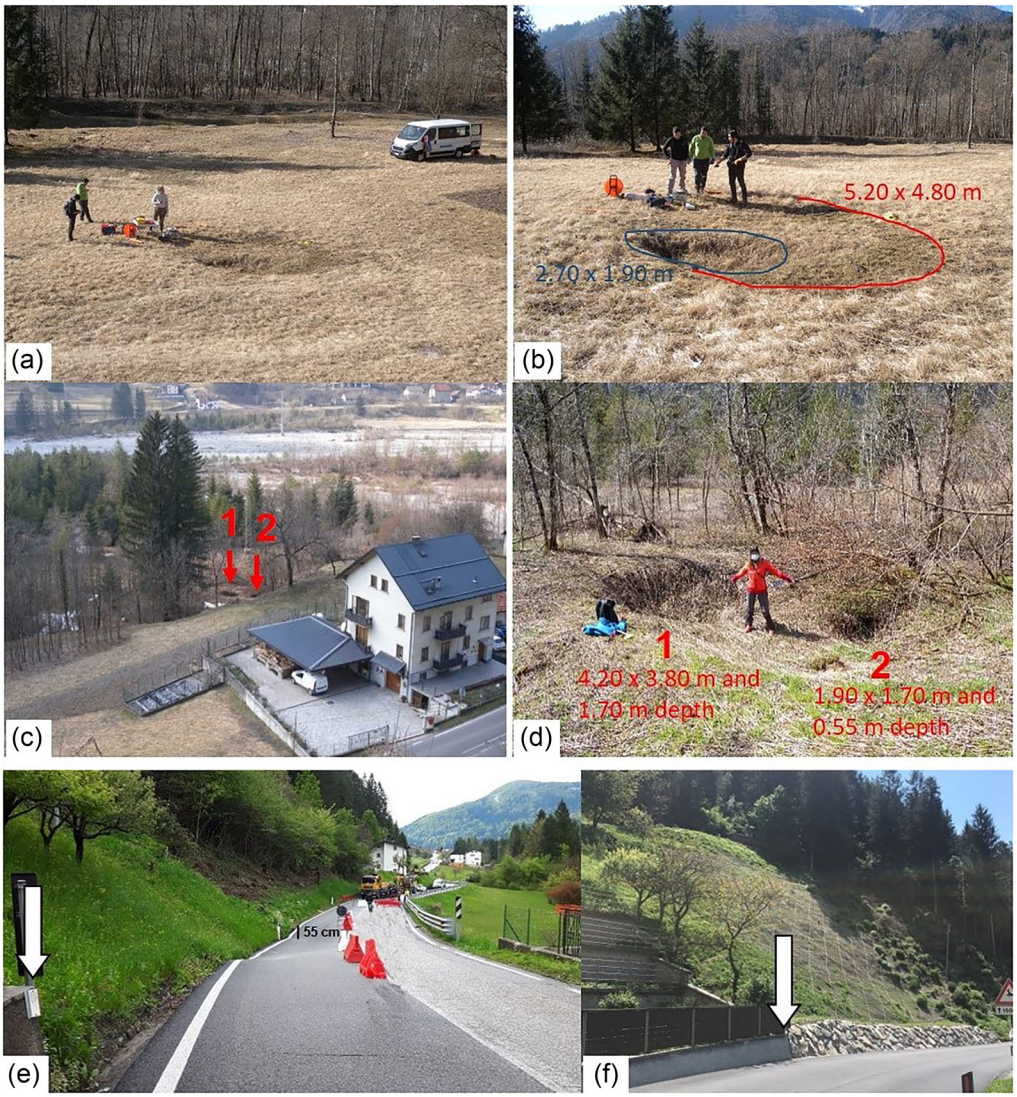

FIGURE 2 Sinkholes in the hamlet of Baus (a–d) with their approximate dimensions. Photo (a) and (b) from February 13, 2020, photo (c) from March 13, 2021 and photo (d) from April 16, 2021. Photographs (e) and (f) (by Dr. Caproni, geologist) documenting the instability phenomenon which occurred on regional road 355 on May 11, 2017 (e) and works done in order to make the road safer (f). Vertical arrows highlight the same location on the two photographs collected in different moments (just after the event (e), and after repairs (f)).

TABLE 1 Geophysical methods used, geometries and acquisition parameters.

Geophysical method	Equipment	Geometry	Main acquisition parameters
ERT Profile 1, 2 and 3	Syscal Pro (Iris) 48 or 72 electrodes	2 profiles 94 m long, 1 profile 142 m long 2 m electrode spacing	Wenner and Wenner–Schlumberger electrode configurations
Refraction seismic Profile 1,2	Geode (Geometrics) 24 channels 5 kg sledgehammer shooting on a metal plate Vertical 14 Hz geophones	2 profiles 102 m long 12 conjugated shots; 24, 4 m spaced vertical geophones	Vertical stacking: 4; 1 s trace length, 0.25 ms sampling interval
GPR Profile 1	ProEx (Malå Geosciences) 250 and 800 MHz shielded antennas	2 profiles along the same path, 96 m long Trace interval: 5 cm	Vertical stacking: 16; trace length: 191.24 ns (250 MHz) and 104.17 ns (800 MHz)
Electromagnetic induction (FDEM) Profile 1	CMD explorer (GF instruments)	2 profiles along the same path, 96 m long	High depth acquisition mode; spatial sampling 1 s

Abbreviations: ERT, electrical resistivity tomography; FDEM, frequency domain electromagnetic; GPR, Ground Penetrating Radar.

18730604, 2023, 5, Downloaded from https://onlinelibrary.wiley.com/doi/10.1002/nsg.12261 by Universita Di Trieste, Wiley Online Library on [28/01/2025]. See the Terms and Conditions (https://onlinelibrary.wiley.com/terms-and-conditions) on Wiley Online Library for rules of use; OA articles are governed by the applicable Creative Commons License

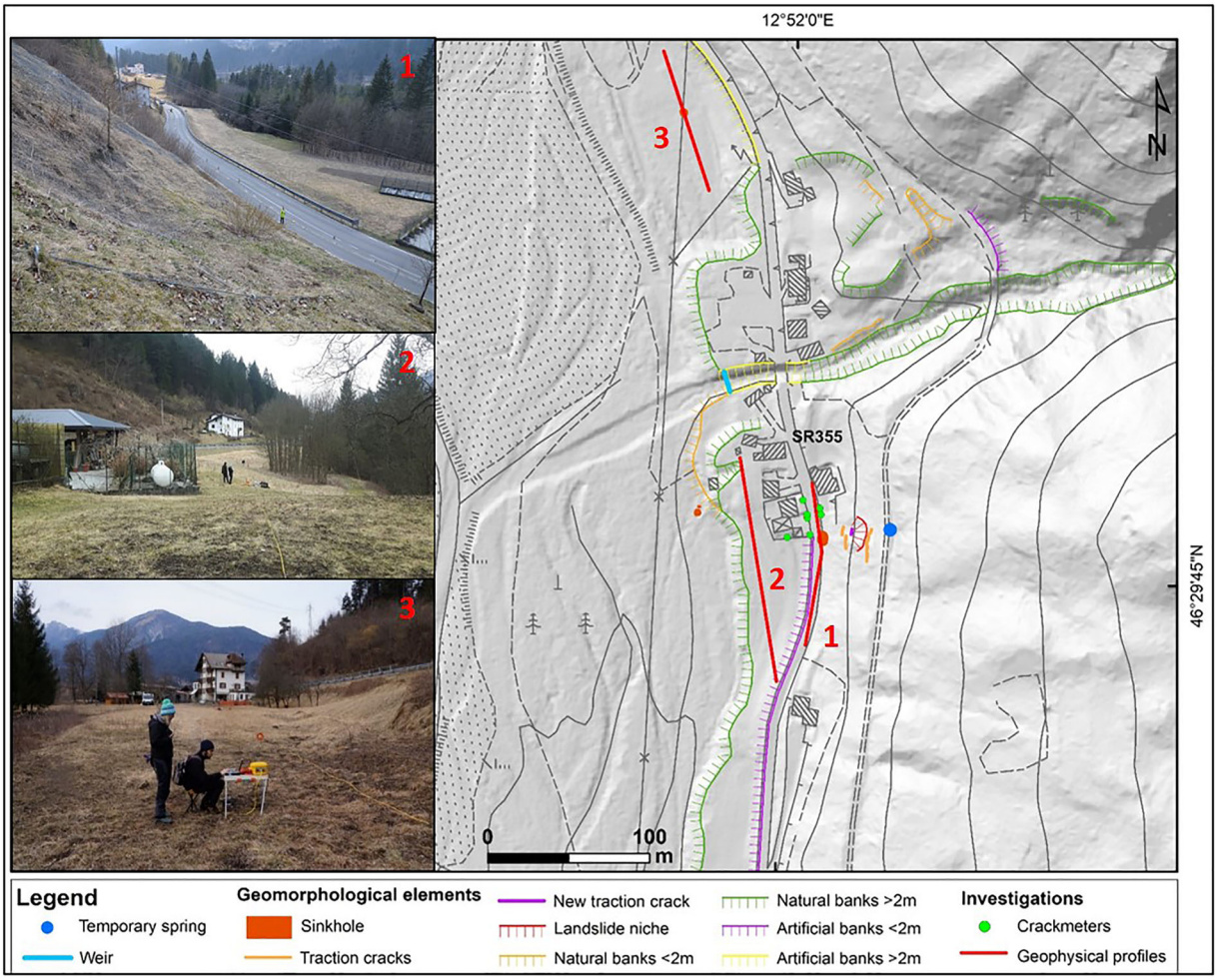

FIGURE 3 Geomorphological map of the hamlet of Baus with the location of the crack-metres and the geophysical profiles. Photos 1, 2 and 3 show the geophysical acquisition of the three profiles and are named accordingly.

the measure obtained with direct and reciprocal electrode combinations, analysing the standard deviation between data repeated with the same quadrupoles, which was always very low. FDEM data were registered first in N–S direction and then in the opposite one in order to guarantee a sufficient statistical repetitiveness. In the RS survey, we set a constant vertical stacking equal to 4 (i.e., four repeated shots for each source location) thus increasing the signal-to-noise ratio by minimizing the random noise level and in turn making the first breaks easier to detect, even for large offsets.

As far as the inversion misfit, it was equal to a maximum of 2 ms for RS after 6 iterations, to 4.3 root mean squared (RMS) mean percentage error for ERT after 5 iterations and to 1.1 RMS mean percentage error for FDEM after 10 iterations. GPR data were collected with 250 MHz and 800 MHz central frequencies shielded antennas to improve both the penetration depth and the attainable resolution. A standard processing is applied considering a constant EM velocity field equal to 0.08 m/ns obtained as a mean value of dedicated diffraction hyperbolas fitting (see, Table 2 to further processing details).

RESULTS

Among all the CM recorded data, only the CM1 showed an initial distensive E–W trend of about 7 mm. The installation was initially done by using only glue and, in February 2018, a particularly intense snowfall detached some of the CM (CM1, CM2 and CM3). The CMs were subsequently reinstalled using screws to fix the devices and since that day only sub-millimetric movements have been recorded.

Regarding geophysical surveys, at first, we considered the RS and ERT profiles crossing the former sinkhole area (Figure 3–Profile 1) in order to highlight subsurface vertical and lateral variations up to a depth of about 30 m. Note that in the sinkhole area, the extensive works done to restore the road encompassed excavations and filling with blocks of rocks and gravel up to

18730604, 2023, 5, Downloaded from https://onlinelibrary.wiley.com/doi/10.1002/nsg.12261 by Universita Di Trieste, Wiley Online Library on [28/01/2025]. See the Terms and Conditions (https://onlinelibrary.wiley.com/terms-and-conditions) on Wiley Online Library for rules of use; OA articles are governed by the applicable Creative Commons License

a depth of 3–4 m. In addition, a borehole was drilled approximately at the centre of the sinkhole. Unluckily, a detailed stratigraphy is not available, but eyewitnesses reported that the drilling reached a depth of 10 m from the surface without intercepting cavities or the bedrock, but only sandy and silty gravel sediments.

Using this information as background, it is possible to interpret the highest real resistivity gradient variations highlighted in Figure 4b. The black dotted line marks a laterally quite continuous transition between a shallow low resistivity level and a medium-to-high resistivity level (values between about 300 Ω m and 1000 Ω m). Below such a layer, at about 5–6 m from the surface, there is a sub-horizontal sharp transition towards low resistive materials (values <150 Ω m). At 12–14 m the resistivity increases again (yellow dotted line). By analysing the corresponding RS profile (Figure 4a) we note a good correspondence to the shallowest interface that divides materials having a P-wave velocity below 800 m/s from deeper materials with velocities ranging from 800 m/s to 1200 m/s. The transition marked by the white dotted line is not apparent on the seismic panel, whereas the deepest horizon can be interpreted as the transition to materials with velocities above 2000 m/s.

By combining all the described elements we can interpret the shallower layer as low compaction fine materials also related to road construction; the high resistivity and intermediate seismic velocity layer as coarser sediments (locally with blocks); the layer between white and yellow dotted lines is most probably composed of similar materials as above, but water saturated as evidenced by the low and homogeneous resistivity values and by the absence of an abrupt transition in seismic velocity which has values close to 1500 m/s. The deepest high resistivity and high-velocity layer can be interpreted as the bedrock, which, from the seismic velocity profile has only limited lateral variations (at N and S limits of the sections the lower velocities are most probably just inversion artefacts).

Profile 2 is located 20–40 m to the W from Profile 1 (Figure 3), and both resistivity and P-wave velocity ranges are similar to Profile 1. However, there are some peculiar features (Figure 4c–d) in the distribution of both parameters. The 2D resistivity section (Figure 4d) shows an uppermost relatively low resistive layer just 1–2 m thick (200–400 Ω m) overlaying a layer with resistivity exceeding 1000 Ω m, followed by lower resistive materials (100–400 Ω m). In the northern portion of the profile, the situation is different; in fact, at the surface, there are resistivities higher than 1000 Ω m, which continue in-depth and there is a sharp lateral resistivity variation (marked by the black dashed segment in Figure 4d). If we superimpose the most apparent resistivity change locations on the seismic velocity profile (Figure 4c), whereas there are no relevant variations at the locations of the shallowest two horizons (black and white dotted lines), the deeper horizon (yellow dotted line) and the lateral transition correspond to remarkable increases in seismic velocity. Therefore, we interpreted: the shallower layer as low compaction silty–sandy materials; the high resistivity and intermediate seismic velocity layer as coarser materials similarly to Profile 1; the layer between

TABLE 2 Details about software, algorithms and parameters applied for geophysical data analysis, processing and inversion.

Geophysical method	Software used	Main processing/inversion algorithms	Main processing/inversion parameters
ERT	ProsysII (3.14), Res2Dinv (4.9), ErtLab Studio	Damped least-squares (Marquard) inversion Smoothness constrained least-squared algorithm with Tikhonov model regularization and tetrahedral finite elements inversion (LaBrecque et al., 1999)	Direct and reciprocal data check. No resistivity model constraints. Convergence limit 5% of absolute variation
Refraction seismic	SeisImager (3.14)	Automated first beak picking (with manual check) Combined inversion methods (reciprocal and travel time tomography approaches)	12 shot gathers No vertical smoothing, no minimum and maximum velocity constraints Difference between observed and calculated travel times always below 2 ms
GPR	Prism2 (2.70.03) Matlab scripts	Zero-time correction, Background removal, bandpass filtering, Velocity analysis by hyperbola fitting, exponential amplitude recovery, dominant frequency analysis, hyperbolic summation migration and depth conversion	Bandpass corner frequencies: 50–80–450–550 MHz (250 MHz antenna); 200–300–1200–1400 MHz (800 MHz antenna) Velocity used for migration, and depth conversion: 8 cm/ns
Electromagnetic induction (FDEM)	EM4soil (3.05)	1D laterally constrained inversion. No resistivity range constraints	

Abbreviations: ERT, electrical resistivity tomography; FDEM, frequency domain electromagnetic; GPR, Ground Penetrating Radar.

18730604, 2023, 5, Downloaded from https://onlinelibrary.wiley.com/doi/10.1002/nsg.12261 by Universita Di Trieste, Wiley Online Library on [28/01/2025]. See the Terms and Conditions (https://onlinelibrary.wiley.com/terms-and-conditions) on Wiley Online Library for rules of use; OA articles are governed by the applicable Creative Commons License

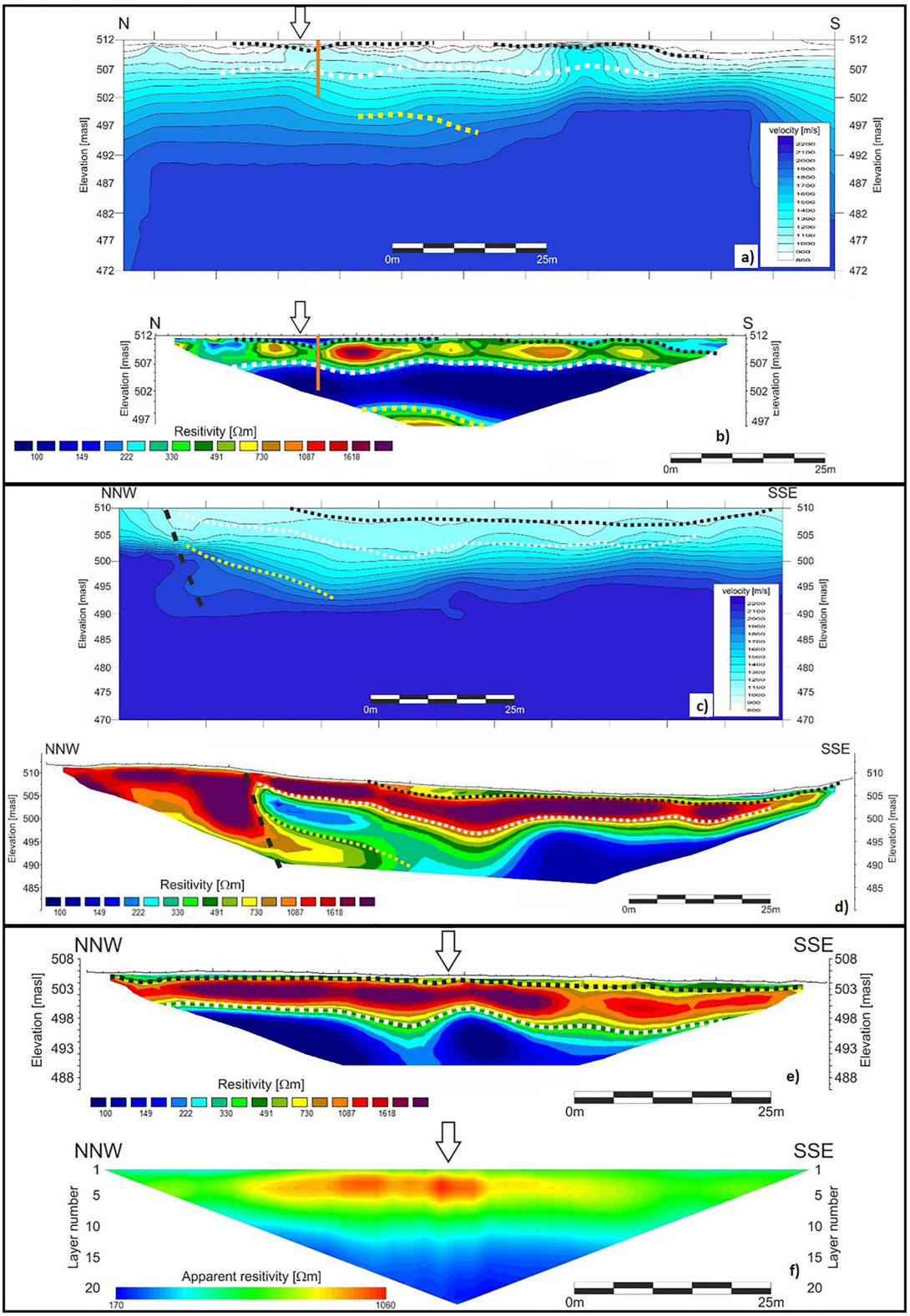

FIGURE 4 (a) RS P wave velocity along Profile 1; (b) ERT inverted resistivity along Profile 1. Vertical white arrows mark the approximate centre of the former sinkhole; black, white and yellow dotted lines highlight the larger resistivity gradients and have also been superimposed on the RS profile. The orange vertical segment depicts the location and depth of a borehole drilled soon after the sinkhole occurrence. All profiles have the same vertical and horizontal scales. (c) RS velocity along Profile 2; (d) ERT inverted resistivity along Profile 2. Black, white and yellow dotted lines highlight the larger resistivity gradients, while the black dashed segment marks the location of an abrupt lateral change. All lines have also been superimposed on the RS profile. All profiles have the same vertical and horizontal scales. (e) ERT inverted resistivity along Profile 3. Black and white dotted lines highlight the larger resistivity gradients. (f) apparent resistivity profile. Vertical arrows indicate the location of the newly developed sinkhole. Please see text for further details. For the location of Profile 1, 2 and 3 see Figure 3.

18730604, 2023, 5, Downloaded from https://onlinelibrary.wiley.com/doi/10.1002/nsg.12261 by Universita Di Trieste, Wiley Online Library on [28/01/2025]. See the Terms and Conditions (https://onlinelibrary.wiley.com/terms-and-conditions) on Wiley Online Library for rules of use; OA articles are governed by the applicable Creative Commons License

the white and yellow dotted lines as water-saturated materials. The yellow dotted line is most probably the top of the bedrock. It is interesting to note that the lateral resistivity and seismic velocity variations are located in correspondence to the former sinkhole (about 30 m to the E) and are related to a main geological element. Moreover, we can note a morphological change from almost constant elevations further north from this point to a lower elevation to the south (Figure 4d). We cannot exclude that this lateral variation is due to a tectonic element responsible for the shallowing of the bedrock to the N, but it could also be a filled erosional channel. The localized low resistivity zone to the E of the sharp lateral transition can be attributed to a water flow from the mountain to the river, possibly acting as a triggering or pushing cause for the sinkhole occurrence.

In order to better understand the geological and hydrological backgrounds in the area of the former sinkhole, we extended our analyses to Profile 3 collected about 150 m to the N and crossing a newly developed depression (Figure 3–Profile 3). The resistivity profile does not show relevant lateral variations, whereas the vertical resistivity distribution is very similar to that already described for the southern part of Profile 2, as well as the resistivity range. The lowest resistivity zone can also be interpreted in this case as related to water-saturated sediments which can be linked to the river bed having a mean elevation of 502 m a.s.l. in this area. At the location where the profile crosses the newly developed sinkhole (cover suffosion sinkhole), no relevant resistivity variations can be found on the inverted model (Figure 4e), whereas on the apparent resistivity data (Figure 4f), the highest values of the whole profile are recorded, but no clear 'anomalies' can be detected.

Considering high-resolution and shallow geophysical data (i.e. GPR and FDEM) collected along the road (Figure 5, see Figure 3 for location), some interesting additional features can be noted. From both low and high-frequency GPR data, several horizons are imaged: while to the S of the former sinkhole they are subhorizontal or regularly gently dipping to the S, in the depressed zone (the centre of which is marked by the vertical white arrow in Figure 5a–c) many horizons are concave up, thus depicting local depocentres (marked by red arrows) with general higher dipping for increasing depths. In addition, below the zone in which the sinkhole developed, the electromagnetic attenuation is higher, especially on the 250 MHz profile (light blue texture). Please note that extensive restoration works were done after the sinkhole occurrence in 2017 with excavations and refilling; however, the GPR horizons concavity could suggest movements occurred after the restoration, whereas the high attenuation zone can be interpreted as higher water saturation than the other portions of the profile. Such information can be very helpful, especially when repeated surveys are available because by comparing data collected at different times it is possible to highlight and monitor possible deformations and movements which occurred between the subsequent surveys. For instance, high-frequency GPR data are able to detect horizons and structures even very close to the surface at a decimetric resolution level. In order to follow this approach, positioning at centimetric accuracy is mandatory in order to make it possible to repeat surveys along the same profiles.

FDEM data (Figure 5c) show a quite homogeneous decreasing vertical resistivity trend, except for the northern portion of the profile where medium to low resistivities are detected. The range of resistivities is similar to the one obtained in the corresponding ERT profile (Figure 4c), as well as the resistivity distribution, excluding the shallower portion for which the FDEM method registers high resistivities, whereas ERT images low values. This discrepancy is limited to the shallower layer and can be related to both the intrinsic physical differences between the two techniques and the field operations (see, e.g., Borgatti et al., 2017). In fact, while for the induction method (i.e., FDEM) we moved the coils at a constant elevation equal to one metre above the road, for ERT we drilled 2–3 decimetre deep holes to fix electrodes bypassing the high resistive asphalt cover. In any case, the locations of transitions between high-to-medium and medium-to-low resistivities obtained by FDEM are similar to the ones resulting from the ERT survey, as well as the overall correspondence between FDEM and GPR results, even at a different resolution level (Figure 5).

DISCUSSION

Sinkholes can generally be considered elusive structures due to the intrinsic difficulty in detecting the precursor signs which come before their occurrence. An emblematic case is the one just happened (May 21, 2022) in a small village in NE Italy (Rosso, 2022). A cover collapse sinkhole of about 18 m in diameter and 15 m in-depth suddenly occurred on a terrace where only a few hours before the landowner had crossed without noticing any evidence of a further sudden collapse. This event is just one of the several examples that we could cite but points to how little knowledge there is regarding the predictability of these phenomena. In Italy, scientists are currently mainly focused on cataloguing (Vennari & Parise, 2022), and no monitoring is taking place as well as on the identification of possible future occurrences in terms of evolution and susceptibility (Calligaris et al., 2017b; Ciotoli et al., 2015). The methodological approach presented here is preliminary to an investigation protocol aimed at identifying,

18730604, 2023, 5, Downloaded from https://onlinelibrary.wiley.com/doi/10.1002/nsg.12261 by Universita Di Trieste, Wiley Online Library on [28/01/2025]. See the Terms and Conditions (https://onlinelibrary.wiley.com/terms-and-conditions) on Wiley Online Library for rules of use; OA articles are governed by the applicable Creative Commons License

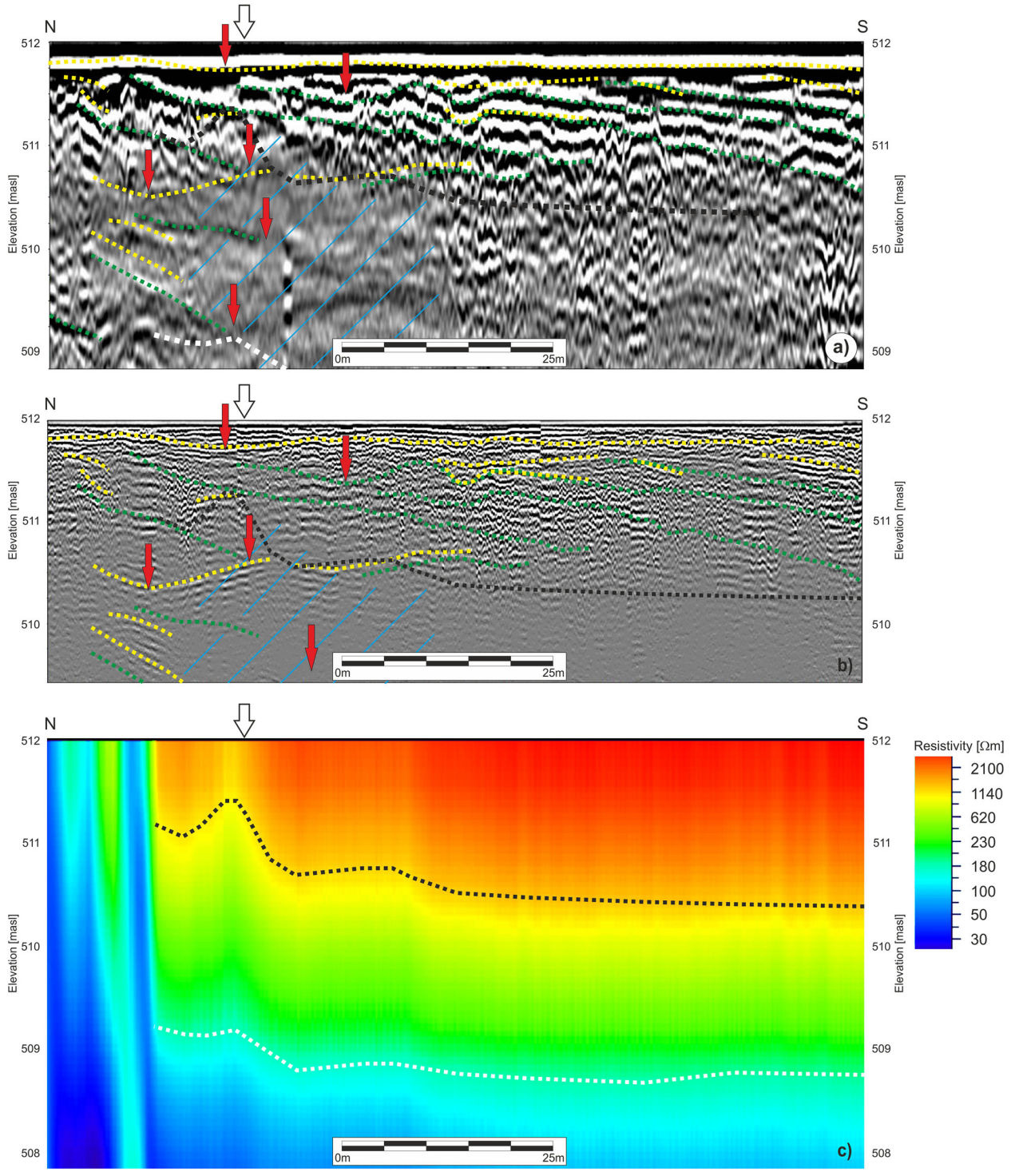

FIGURE 5 (a) 250 MHz Ground Penetrating Radar (GPR) profile; (b) 800 MHz GPR profile; (c) frequency domain electromagnetic (FDEM) profile. White arrows point to the centre of the sinkhole; red arrows highlight depocentres; red and yellow dotted lines follow the main GPR horizons interpreted respectively on 250 and 800 MHz profiles and are superimposed on both for a better visual comparison; light blue texture marks a higher attenuation zone on GPR sections. Black and white dotted lines follow the maximum resistivity gradients as in Figure 4 and are also superimposed on GPR profiles for a better visual comparison. All profiles have the same vertical and horizontal scales. See Figure 3 for profiles location.

18730604, 2023, 5, Downloaded from https://onlinelibrary.wiley.com/doi/10.1002/nsg.12261 by Universita Di Trieste, Wiley Online Library on [28/01/2025]. See the Terms and Conditions (https://onlinelibrary.wiley.com/terms-and-conditions) on Wiley Online Library for rules of use; OA articles are governed by the applicable Creative Commons License

TABLE 3 Summary of some of the most recent papers related to sinkhole investigations in carbonate and evaporite environments.

Type of sinkhole	Involved material	Used approach	Location	Reference
Collapse	Limestone	ERT, seismic tomography, MASW	Thailand	Yordkayhun et al. (2022)
Undefined	Roadway substructure	Seismic tomography	Florida	Wang et al. (2022)
Collapse	Limestone/sandstone	GPR	Brazil	Lago et al. (2022)
Collapse	Carbonate deposits	InSAR and spatial clustering analysis (DBSCAN)	West-central Florida	Talib et al. (2022)
Cover collapse	Mudstone, muddy limestone	MERM	Hunan province, China	Pan et al. (2022)
Collapse	Limestone	ERT	Thailand	Arjwech et al. (2021)
Collapse	Travertine	Altimetry, magnetic, microgravity, seismic refraction, electrical resistivity and soli gas surveys	Italy	Argentieri et al. (2015)
Cover collapse	Limestone/quaternary	GPR and electrical resistivity tomography	Algeria	Nouioua et al. (2013)
Undefined	Triassic brecciated dolomitic limestone and Cretaceous slate/alluvial deposits	2D- and 3D-electrical resistivity tomography, microgravity and single-station seismic noise measures	Italy	Pazzi et al. (2018)
Sagging vs. collapse	Evaporites	GPR	Spain	Rodriguez et al. (2014)
Collapse	Evaporites in urban area	Trenching, GPR, ERT and high precision levelling	Spain	Sevil et al. (2017)
All types	Evaporite karst	Trenching, geophysical investigations	Spain	Gutierréz et al. (2018)

Abbreviations: ERT, electrical resistivity tomography; GPR, Ground Penetrating Radar; MERM, multi-electrode resistivity method.

characterizing and monitoring such phenomena in heavily infrastructured environments. From this perspective, 'the use' of small well-known areas as test sites could also be extremely useful to implement, check and validate a multi-technique non-invasive approach, with short acquisition periods and moderate acquisition costs, not negligible when scheduling long-term monitoring.

At the international level, in those parts of the world where these phenomena are present, in the recent years ever more detailed investigations have been done in order to detect and outline these sometimes catastrophic events (Table 3).

The geophysical approaches used have been applied mainly on non-evaporitic lithologies and gave results of excellent quality with regards to sinkhole sagging and collapsing. There are few examples of evaporites and even fewer of evaporites mantled by quaternary deposits. This is the case of the sinkholes found in the FVG integrating ERT, RS, GPR and FDEM, where large voids were not imaged by the applied geophysical techniques.

As also reported in other similar studies (e.g., Busetti et al., 2020; Gutiérrez et al., 2011; Zini et al., 2015) this is an interesting indication for sinkhole origin, classification and evolution. In fact, although there are many examples of caves detected at different scales by geophysical surveys (e.g., Carbonel et al., 2015; Giampaolo et al., 2016; Youssef et al., 2012), cover collapse and cover suffosion sinkholes are more elusive structures having a less peculiar geophysical signature. However, repeated ERT and/or FDEM surveys could be very useful in the detection of the formation of relatively large voids and, more importantly, to highlight local water filling time variations that can be serious triggering causes to activate or reactivate sinkholes. On the other hand, repeated GPR surveys may be able to detect even small changes and movements by comparing the same horizon locations at different temporal steps. The latter can be done at first by just a visual comparison, but improved results can be achieved exploiting the various attributes of GPR in particular related to phase and frequency or texture attributes (Zhao et al., 2016). GPR has shown high potential in the early imaging of failures, voids and defects of road pavements (e.g., Saarenketo & Scullion,2000; Thitimakorn et al., 2016). Similarly, GPR could be used in this context to highlight centimetric–decimetric voids formed just below the binder/foundation/subgrade thanks to its very high resolution.

In the present case, the integration of geomorphological analysis, crack monitoring, and combined

18730604, 2023, 5, Downloaded from https://onlinelibrary.wiley.com/doi/10.1002/nsg.12261 by Universita Di Trieste, Wiley Online Library on [28/01/2025]. See the Terms and Conditions (https://onlinelibrary.wiley.com/terms-and-conditions) on Wiley Online Library for rules of use; OA articles are governed by the applicable Creative Commons License

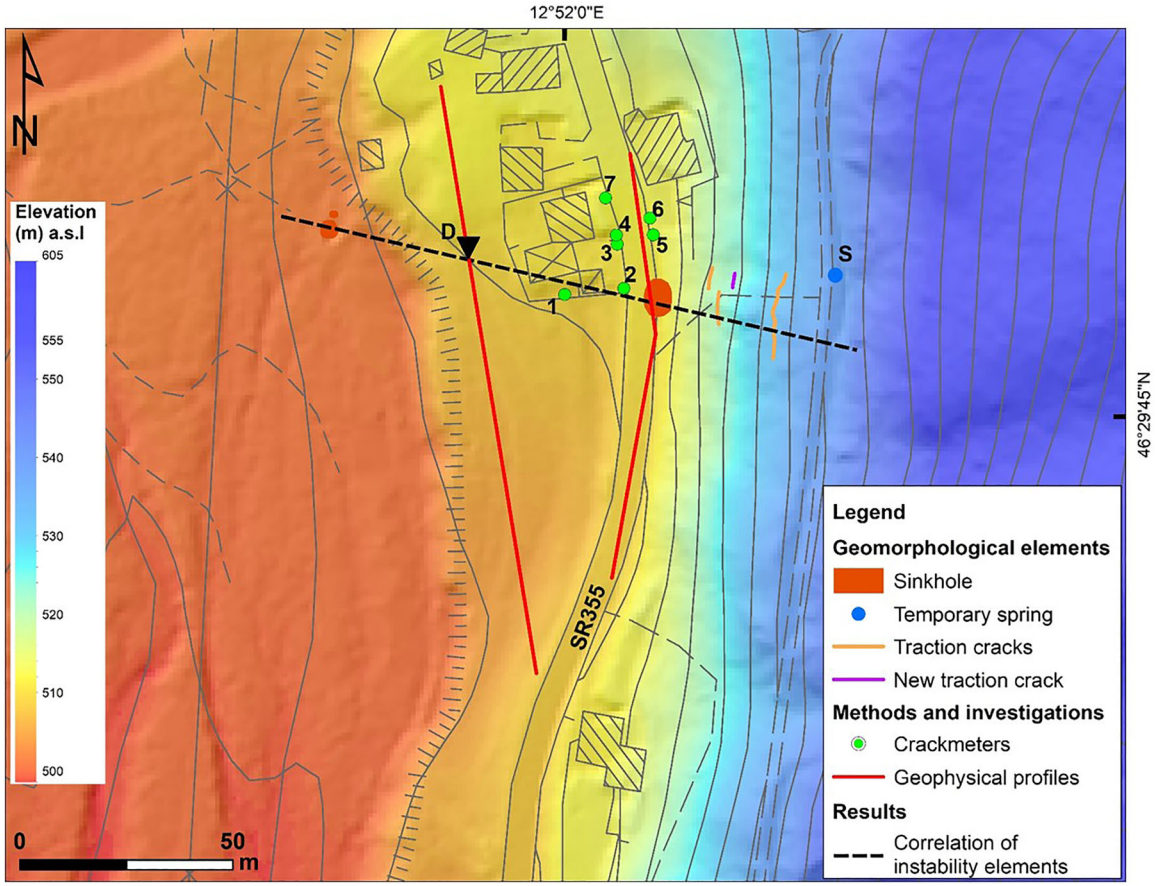

FIGURE 6 Spatial correlation of sinkholes, ground and infrastructure cracks and hydrological elements in the study area. Green points represent the crack-metres (on walls and pavements); orange and purple lines depict main ground fractures; D refers to the location of the abrupt lateral discontinuity as highlighted by a geophysics analysis (Figure 4); S label marks a temporary spring. The black dotted segment spatially links the previous elements. See text for further details and discussion.

multi-resolution geophysical techniques, allowed for a broader examination of the sinkhole in a wider context (Figure 6). However, for analysis at the scale of several square kilometres, other techniques and acquisition protocols can be essential such as, for instance, airborne geophysics combined with dedicated LiDAR and InSAR analyses.

We found that there is a straight ESE–WNW correlation between the main and the other two sinkholes, as well as with the abrupt lateral discontinuity imaged by ERT and RS data (letter 'D' in Figure 6). Traction cracks developed along the same line-up and there is a spring located only a few metres to the North. This ESE–WNW trend can be correlated with a main groundwater path acting as a cause or concurrent cause of the sinkhole development. This demonstrates that it is not sufficient to focus on the zone where a specific event occurred, but it is mandatory to broaden the area of analysis taking into consideration a multi-scale, multi-technique, and integrated approach.

None of the analyses showed evidence of relatively large caves and agree that in this area sinkholes are not linked to the bedrock depth: a deeper bedrock does not mean a safer area. The presence of a groundwater path represents a triggering factor by increasing local karstification and favouring sinkhole processes. The sinkhole could start as cover suffosion coupled with downward migration of the cover material into pipes present in the bedrock enlarged by solution (Gutiérrez et al., 2008) (Figure 7a). The presence of more competent layers on the shallower portion of the stratigraphic profile that, in the case of the damaged road is represented by the road pavement and by a layer of more cohesive cover, allows for the formation of a void beneath (Figure 7b) without any visible evidence of what is occurring below the surface. With the evolution of the suffosion sinkhole, the void under the anthropogenic cover enlarges up to the occurrence of a collapse (Figure 7c).

A situation like the one just described is a definitive risk in an urban environment, especially due to the lack of precursor signs on the surface. Following the evolution of the phenomena by the use of a geophysical integrated approach would not prevent collapses but may prevent

18730604, 2023, 5, Downloaded from https://onlinelibrary.wiley.com/doi/10.1002/nsg.12261 by Universita Di Trieste, Wiley Online Library on [28/01/2025]. See the Terms and Conditions (https://onlinelibrary.wiley.com/terms-and-conditions) on Wiley Online Library for rules of use; OA articles are governed by the applicable Creative Commons License

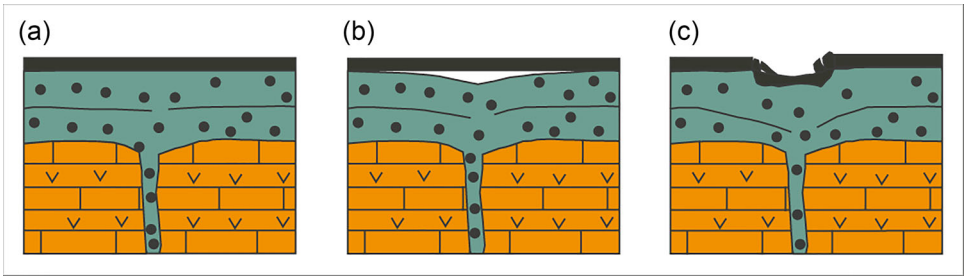

FIGURE 7 Subsidence mechanism generating the occurred sinkhole. The thick black line corresponds to the man-made cover, the green colour represents the granular sediments and the evaporitic bedrock is represented in orange. (a) Migration of particles through dissolution conduits in an early stage; (b) migration of particles through dissolution conduits and void formation beneath the man-made cover; (c) collapse of the man-made cover.

possible future road disasters. Moreover, if the problem is correctly identified, a monitoring programme can be design in order to detect possible precursors of large failures.

CONCLUSIONS

The presence of evaporitic bedrock is certainly the main predisposing factor for sinkhole occurrence in infrastructured areas and it has to be monitored over time given its fast dissolution (Calligaris et al., 2020) in order to avoid the occurrence of sudden collapses which could represent a serious risk for people and man-made structures. On a test site area located in the extreme NE corner of the Italian peninsula, a joint geophysical approach was applied in order to tune an integrated monitoring method in a site where a sinkhole formed in 2017 causing an interruption to traffic on a major roadway. From this study emerged the importance of applying and integrating different methods at a time to clarify the imaged geological model and to explain the sinkhole occurrence. Electrical and seismic tomographies allow for the image of the subsurface down to a depth exceeding 15–20 m, whereas GPR and EM techniques imaged the shallowest portion down to about 4–5 m from the surface. Repeated ERT and/or FDEM surveys could be very useful to detect the formation of relatively large voids and, even more important, to highlight local water filling time variations that can be significant triggering causes to activate or reactivate sinkholes. Repeated use of GPR could image superficial void of decimetric dimension, and this could help monitor the road over time not in terms of preventing a collapse, but to avoid possible future disasters on roads. In the present case, the formed sinkhole occurred due to the presence of the evaporitic bedrock which had been heavily karstified by the circulation of the ground and spring waters. The phenomenon likely has a complex genesis and the presence of a more competent layer at the surface, that is the road, did not allow for researchers to follow the ongoing natural process of sinkhole formation due to the asphalt cover.

ACKNOWLEDGEMENTS

The authors would like to acknowledge the functionaries of the Geological Survey of the Friuli Venezia Giulia (FVG) Region: Chiara Piano, Franco Liuzzi and Fabrizio Kranitz, the scientific coordinators from the various joint projects with the University of Trieste, Dept. of Mathematics and Geosciences. The Authors wish to thank the functionaries from FVG Strade, Alessandra Biondin and Alessio Vidoni, who facilitated the road closures necessary to conduct our investigations. We thank Dario Saponaro and Alessandra Lanzoni for data collection in the field. The associate editor Sebastian Uhlemann and two anonymous reviewers are acknowledged for their advisable comments and suggestions.

DATA AVAILABILITY STATEMENT

The data sets generated and analysed during the current study are available from the corresponding author on reasonable request or from Geological Survey of the Friuli Venezia Giulia Region (Italy).

REFERENCES

Argentieri, A., Carluccio, R., Cecchini, F., Chiappini, M., Ciotoli, G., De Ritis, R. et al. (2015) Early stage sinkhole formation in the Acque Albule basin of central Italy from geophysical and geochemical observations. *Engineering Geology*, 191, 36–47. https://doi.org/10.1016/j.enggeo.2015.03.010

Arjwech, R., Ruansorn, T., Schulmeister, M., Everett, M.E., Thitimakorn, T., Pondthai, P. et al. (2021) Protection of electricity transmission infrastructure from sinkhole hazard based on electrical resistivity tomography. *Engineering Geology*, 293, 106318. https://doi.org/10.1016/j.enggeo.2021.106318

Baer, G., Magen, Y., Nof, R., Raz, E., Lyakhovsky, V. & Shalev, E. (2018) InSAR measurements and viscoelastic modelling of sinkhole precursory subsidence: implications for sinkhole formation, early warning, and sediment properties. *Journal of Geophysical Research-Earth Surface*, 123, 678–693. https://doi.org/10.1002/2017JF004594

Basso, A., Bruno, E., Parise, M. & Pepe, M. (2013) Morphometric analysis of sinkholes in a karst coastal area of southern Apulia (Italy). *Environmental Earth Sciences*, 70, 2545–2559. https://doi.org/10.1007/s12665-013-2297-z

Borgatti, L., Forte, E., Mocnik, A., Zambrini, R., Cervi, F., Martinucci, D. et al. (2017) Detection and characterization of animal burrows within river embankments by means of coupled remote sensing and

18730604, 2023, 5, Downloaded from https://onlinelibrary.wiley.com/doi/10.1002/nsg.12261 by Universita Di Trieste, Wiley Online Library on [28/01/2025]. See the Terms and Conditions (https://onlinelibrary.wiley.com/terms-and-conditions) on Wiley Online Library for rules of use; OA articles are governed by the applicable Creative Commons License

geophysical techniques: lessons from River Panaro (northern Italy). *Engineering Geology*, 226, 30, 277–289. https://doi.org/10.1016/j.enggeo.2017.06.017.

Brinkmann, R., Parise, M. & Dye, D. (2008) Sinkhole distribution in a rapidly developing urban environment: Hillsborough County, Tampa Bay area, Florida. *Engineering Geology*, 99, 169–184. https://doi.org/10.1016/j.enggeo.2007.11.020

Bruno, E., Calcaterra, D. & Parise, M. (2008) Development and morphometry of sinkholes in coastal plains of Apulia, southern Italy: preliminary sinkhole susceptibility assessment. *Engineering Geology*, 99, 198–209. https://doi.org/10.1016/j.enggeo.2007.11.017

Busetti, A., Calligaris, C., Forte, E., Areggi, G., Mocnik, A. & Zini, L. (2020) Non-invasive methodological approach to detect and characterize high-risk sinkholes in urban cover evaporite karst: integrated reflection seismics, PS-InSAR, leveling, 3D-GPR and ancillary data. A NE Italian case study. *Remote Sensing*, 12(22), 3814. https://doi.org/10.3390/rs12223814

Buttrick, D.B. & van Schalkwyk, A. (1998) Hazard and risk assessment for sinkhole formation on dolomite land in South Africa. *Environmental Geology*, 36, 170–178. https://doi.org/10.1007/s002540050333

Calligaris, C., Devoto, S., Zini, L. & Cucchi, F. (2017a) An integrated approach for investigations of ground subsidence phenomena in the Ovaro Village (NE Italy). In: Renard, P. & Bertrand, C. (Eds.) *EuroKarst 2016, Neuchâtel. Advances in karst science*. Cham: Springer, pp. 71–77. https://doi.org/10.1007/978-3-319-45465-8_8

Calligaris, C., Devoto, S. & Zini, L. (2017b) Evaporite sinkholes of the Friuli Venezia Giulia region (NE Italy). *Journal of Maps*, 13(2), 406–414. https://doi.org/10.1080/17445647.2017.1316321

Calligaris, C., Ghezzi, L., Petrini, R., Lenaz, D. & Zini, L. (2019) Evaporite dissolution rate through an on-site experiment into piezometric tubes applied to the real case-study of Quinis (NE Italy). *Geosciences*, 9, 298. https://doi.org/10.3390/geosciences9070298

Calligaris, C., Zini, L., Nisio, S. & Piano, C. (2020) Sinkholes in the Friuli Venezia Giulia Region focus on the evaporites. In: *Applied geology*. Cham: Springer. https://doi.org/10.1007/978-3-030-43953-8_5

Caproni, F. (2017) *Intervento urgente per la sistemazione del dissesto geologico avvenuto al km 11+182 della SR n° 355 "della Val Degano"*. Technical report, p. 16.

Carbonel, D., Rodríguez-Tribaldos, V., Gutiérrez, F., Galve, J.P., Guerrero, J., Zarroca, M. et al. (2015) Investigating a damaging buried sinkhole cluster in an urban area integrating multiple techniques: geomorphological surveys, DInSAR, GPR, ERT, and trenching. *Geomorphology*, 229, 3–16. https://doi.org/10.1016/j.geomorph.2014.02.007

Ciotoli, G., Finoia, M.G., Liperi, L., Meloni, F., Nisio, S., Tonelli, V. et al. (2015) Sinkhole susceptibility map of the Lazio Region, Central Italy. *Journal of Maps*, 12, 287–294. https://doi.org/10.1080/17445647.2015.1014939

Cooper, A.H. (1998) In: Maund, J.G. & Eddleston, M. (Eds.) *Subsidence hazards caused by the dissolution of Permian gypsum in England: geology, investigation and remediation*. London, UK: Geohazards in Engineering Geology, Geological Society of London, pp. 265–275. https://www.lyellcollection.org/doi/10.1144/gsl.eng.1998.015.01.27

Cooper, A.H., Farrant, A.R. & Price, S.J. (2011) The use of karst geomorphology for planning, hazard avoidance and development in Great Britain. *Geomorphology*, 134, 118–131. https://doi.org/10.1016/j.geomorph.2011.06.004

Cucchi, F. & Giorgetti, F. (1997) *Relazione sulle risultanze delle campagne geofisiche e dei rilevamenti geologici eseguiti sul terreno*. Final report. Department of Geological, Environmental and Marine Sciences, University of Trieste, p. 23.

Dahm, T., Kühn, D., Ohrnberger, M., Kröger, J., Wiederhold, H., Reuther, C.-D. et al. (2010) Combining geophysical data sets to study the dynamics of shallow evaporites in urban environments: application to Hamburg, Germany. *Geophysical Journal International*, 181, 154–172. https://doi.org/10.1111/j.1365-246X.2010.04521.x

De Ritis, R., Nardi, A., Materni, V., Venuti, A., Stefanelli, P., Rotella, G. et al. (2020) Multidisciplinary study of subsidence and sinkhole occurrences in the Acque Albule Basin (Roma, Italy). *Earth and Space Science*, 7, e2019EA000870. https://doi.org/10.1029/2019EA000870

De Waele, J., Piccini, L., Columbu, A., Madonia, G., Vattano, M., Calligaris, C. et al. (2017) Evaporite karst in Italy: a review. *International Journal of Speleology*, 46, 137–168. https://doi.org/10.5038/1827-806X.46.2.2107

Delkhahi, B., Nassery, H.R., Vilarrasa, V., Alijani, F. & Ayora, C. (2020) Impacts of natural CO_2 leakage on groundwater chemistry of aquifers from the Hamadan Province, Iran. *International Journal of Greenhouse Gas Control*, 96, 103001. https://doi.org/10.1016/j.ijggc.2020.103001

Desir, G., Gutiérrez, F., Merino, J., Carbonel, D., Benito-Calvo, A., Guerrero, J. et al. (2018) Rapid subsidence in damaging sinkholes: measurement by high-precision leveling and the role of salt dissolution. *Geomorphology*, 303, 393–409. https://doi.org/10.1016/j.geomorph.2017.12.004

Dou, J., Li, X., Yunus, A.P., Paudel, U., Chang, K.-T., Zhu, Z. et al. (2015) Automatic detection of sinkhole collapses at finer resolutions using a multi-component remote sensing approach. *Natural Hazards*, 78, 1021–1044. https://doi.org/10.1007/s11069-015-1756-0

Festa, V., Fiore, A., Parise, M. & Siniscalchi, A. (2012) Sinkhole evolution in the Apulian karst of southern Italy: a case study, with some considerations on sinkhole hazards. *Journal of Cave and Karst Studies*, 74, 137–147. https://doi.org/10.4311/2011JCKS0211

Galve, J.P., Remondo, J. & Gutiérrez, F. (2011) Improving sinkhole hazard models incorporating magnitude-frequency relationships and nearest neighbor analysis. *Geomorphology*, 134, 157–170. https://doi.org/10.1016/j.geomorph.2011.05.020

Galve, J.P., Castañeda, C. & Gutiérrez, F. (2015) Railway track deformation detected by DInSAR over a dissolution-induced subsidence area of the Ebro Valley evaporite karst, Spain. *Natural Hazards and Earth System Sciences*, 3, 3967–3981. https://doi.org/10.5194/nhessd-3-3967-2015

García-Moreno, I. & Mateos, R.M. (2011) Sinkholes related to discontinuous pumping: susceptibility mapping base on geophysical studies. The case of Crestatx (Mallorca, Spain). *Environmental Earth Sciences*, 64, 523–537. https://doi.org/10.1007/s12665-010-0876-9

Giampaolo, V., Capozzoli, L., Grimaldi, S. & Rizzo, E. (2016) Sinkhole risk assessment by ERT: the case study of Sirino Lake (Basilicata, Italy). *Geomorphology*, 253, 1–9. https://doi.org/10.1016/j.geomorph.2015.09.028

Guerrero, J., Sevil, J., Desir, G., Gutiérrez, F., Arnay, A.G., Galve, J.P. et al. (2021) The detection of active sinkholes by airborne differential LiDAR DEMs and InSAR cloud computing tools. *Remote Sensing*, 13, 3261. https://doi.org/10.3390/rs13163261

Gutiérrez, F., Galve, J.P., Guerrero, J., Lucha, P., Cendrero, A., Remondo, J. et al. (2007) The origin, typology, spatial distribution, and detrimental effects of the sinkholes developed in the alluvial evaporite karst of the Ebro River valley downstream Zaragoza City (NE Spain). *Earth Surface Processes Landforms*, 32, 912–928. https://doi.org/10.1002/esp.1456

Gutiérrez, F., Guerrero, J. & Lucha, P. (2008) A genetic classification of sinkholes illustrated from evaporite paleokarst exposures in Spain. *Environmental Geology*, 53, 993–1006. https://doi.org/10.1007/s00254-007-0727-5

Gutiérrez, F., Galve, J.P., Lucha, P., Castañeda, C., Bonachea, J. & Guerrero, J. (2011) Integrating geomorphological mapping, trenching, InSAR and GPR for the identification and characterization of sinkholes in the mantled evaporite karst of the Ebro Valley (NE Spain). *Geomorphology*, 134, 144–156. https://doi.org/10.1016/j.geomorph.2011.01.018

Gutiérrez, F., Parise, M., DeWaele, J. & Jourde, H. (2014) A review on natural and human-induced geohazards and impacts in karst. *Earth*

18730604, 2023, 5, Downloaded from https://onlinelibrary.wiley.com/doi/10.1002/nsg.12261 by Universita Di Trieste, Wiley Online Library on [28/01/2025]. See the Terms and Conditions (https://onlinelibrary.wiley.com/terms-and-conditions) on Wiley Online Library for rules of use; OA articles are governed by the applicable Creative Commons License

Science Reviews, 138, 61–88. https://doi.org/10.1016/j.earscirev.2014.08.002

Gutiérrez, F. (2016) *Sinkhole hazards*. Oxford Research Encyclopedia of Natural Hazard Science. https://doi.org/10.1093/acrefore/9780199389407.013.40

Gutiérrez, F., Zarroca, M., Linares, R., Roqué, C., Carbonel, D., Guerrero, J. et al. (2018) Identifying the boundaries of sinkholes and subsidence areas via trenching and establishing setback distances. *Engineering Geology*, 233, 255–268. https://doi.org/10.1016/j.enggeo.2017.12.015

Intrieri, E., Gigli, G., Nocentini, M., Lombardi, L., Mugnai, F., Fidolini, F. et al. (2015) Sinkhole monitoring and early warning: an experimental and successful GB-InSAR application. *Geomorphology*, 241, 304–314. https://doi.org/10.1016/j.geomorph.2015.04.018

Jones, C.E. & Blom, R.G. (2014) Bayou Corne, Louisiana, sinkhole: precursory deformation measured by radar interferometry. *Geology*, 42, 111–114. https://doi.org/10.1130/G34972.1

Karimi, H. & Taheri, K. (2010) Hazards and mechanism of sinkholes on Kabudar Ahang and Famenin plains of Hamadan, Iran. *Natural Hazards*, 55(2), 481–499. https://doi.org/10.1007/s11069-010-9541-6

Kersten, T., Kobe, M., Gabriel, G., Timmen, L., Schon, S. & Vogel, D. (2017) Geodetic monitoring of subrosion-induced subsidence processes in urban areas. *Journal of Applied Geodesy*, 11, 21–29. https://doi.org/10.1515/jag-2016-0029

Kim, Y.J., Nam, B.H. & Youn, H. (2019) Sinkhole detection and characterization using LiDAR-derived DEM with logistic regression. *Remote Sensing*, 11, 1592. https://doi.org/10.3390/rs11131592

Kobe, M., Gabriel, G., Weise, A. & Vogel, D. (2019) Time-lapse gravity and levelling surveys reveal mass loss and ongoing subsidence in the urban subrosion-prone area of Bad Frankenhausen, Germany. *Solid Earth*, 10(3), 599–619. https://doi.org/10.5194/se-10-599-2019

Koutepov, V.M., Mironov, O.K. & Tolmachev, V.V. (2008) Assessment of suffosion-related hazards in karst areas using GIS technology. *Environmental Geology*, 54, 957–962. https://doi.org/10.1007/s00254-007-0888-2

Krawczyk, C.M., Polom, U., Trabs, S. & Dahm, T. (2012) Sinkholes in the city of Hamburg-New urban shear-wave reflection seismic system enables high-resolution imaging of subrosion structures. *Journal of Applied Geophysics*, 78, 133–143. https://doi.org/10.1016/j.jappgeo.2011.02.003

Kühn, D., Ohrnberger, M. & Dahm, T. (2011) Imaging a shallow salt diapir using ambient seismic vibrations beneath the densely built-up city area of Hamburg, Northern Germany. *Journal of Seismology*, 15, 507–531, https://doi.org/10.1007/s10950-011-9234-y

Kuniansky, E.L., Weary, D.L. & Kaufmann, J.E. (2016) The current status of mapping karst areas and availability of public sinkhole-risk resources in karst terrains of the United States. *Hydrogeology Journal*, 24, 613–624. https://doi.org/10.1007/s10040-015-1333-3

LaBrecque, D., Morelli, G., Daily, W., Ramirez, A. & Lundegard, P. (1999) Occam's inversion of 3D electrical resistivity tomography. In: Oristaglio, M., Spies, B. & Cooper, M.R. (Eds.) *Three dimensional electromagnetics*. Tulsa, Oklahoma: Society of Exploration Geophysicists, pp. 575–590.

Lago, A.L., Borges, W.R., Barros, J.S. & de Sousa Amaral, E. (2022) GPR application for the characterization of sinkholes in Teresina, Brazil. *Environmental Earth Sciences*, 81, 132. https://doi.org/10.1007/s12665-022-10265-4

Malehmir, A., Socco, L.V., Bastani, M., Krawczyk, C.M., Pfaffhuber, A.A., Miller, R.D. et al. (2016). Near-surface geophysical characterization of areas prone to natural Hazards: a review of the current and perspective on the future. *Advances in Geophysics*, 57, 51–146. https://doi.org/10.1016/bs.agph.2016.08.001

Malinowska, A.A., Witkowski, W.T., Hejmanowski, R., Chang, L., van Leijen, F.J. & Hanssen, R.F. (2019) Sinkhole occurrence monitoring over shallow abandoned coal mines with satellite-based persistent scatterer interferometry. *Engineering Geology*, 262, 105336. https://doi.org/10.1016/j.enggeo.2019.105336

Margiotta, S., Negri, S., Parise, M. & Valloni, R. (2012) Mapping the susceptibility to sinkholes in coastal areas, based on stratigraphy, geomorphology and geophysics. *Natural Hazards*, 62, 657–676. https://doi.org/10.1007/s11069-012-0100-1

Martinotti, M.E., Pisano, L., Marchesini, I., Rossi, M., Peruccacci, S., Brunetti, M.T. et al. (2017) Landslides, floods and sinkholes in a karst environment: the 1–6 September 2014 Gargano event, southern Italy. *Natural Hazards and Earth System Sciences*, 17, 467–480. https://doi.org/10.5194/nhess-17-467-2017

Nisio, S. (2008) I sinkholes nelle altre regioni. *Memorie Descrittive della Carta Geologica d'Italia*, 85, 419–426. (In Italian)

Nouioua, I., Rouabhia, A., Fehdi, C., Boukelloul, M.L., Gadri, L., Chabou, D. et al. (2013) The application of GPR and electrical resistivity tomography as useful tools in detection of sinkholes in the Cheria Basin (northeast of Algeria). *Environmental Earth Sciences*, 68, 1661–1672. https://doi.org/10.1007/s12665-012-1859-9

Oliver-Cabrera, T., Wdowinski, S., Kruse, S. & Robinson, T. (2020) InSAR detection of localized subsidence induced by sinkhole activity in suburban West-Central Florida. *Proceeding of the International Association of Hydrological Sciences*, 382, 155–159. https://doi.org/10.5194/piahs-382-155-2020

Orhan, O., Oliver-Cabrera, T., Wdowinski, S., Yalvac, S. & Yakar, M. (2021) Land subsidence and its relations with sinkhole activity in Karapınar region, Turkey: a multi-sensor InSAR time series study. *Sensors*, 21, 774. https://doi.org/10.3390/s21030774

Pan, Z., Chen, X., Yang, X., Song, Y., Ban, R. & Zhang, M. (2022) Formation mechanism analysis of cover collapse sinkholes in Wugaishan Town, Chenzhou City, Hunan province, China. *Environmental Earth Sciences*, 81, 48. https://doi.org/10.1007/s12665-022-10171-9

Panno, S.V. & Luman, D.E. (2013) Mapping palimpsest karst features on the Illinois sinkhole plain using historical aerial photography. *Carbonates and Evaporites*, 28, 201–214. https://doi.org/10.1007/s13146-012-0107-4

Parise, M., Qiriazi, P. & Sala, S. (2004) Natural and anthropogenic hazards in karst areas of Albania. *Natural Hazards and Earth System Sciences*, 4, 569–581. https://doi.org/10.5194/nhess-4-569-2004

Parise, M. (2015) A procedure for evaluating the susceptibility to natural and anthropogenic sinkholes. *Georisk*, 9, 272–285. https://doi.org/10.1080/17499518.2015.1045002

Paukstys, B., Cooper, A.H. & Arustiene, J. (1999) Planning for gypsum geohazards in Lithuania and England. *Engineering Geology*, 52, 93–103. https://doi.org/10.1016/S0013-7952(98)00061-1

Pazzi, V., Di Filippo, M., Di Nezzac, M., Carlàa, T., Bardia, F., Marinia, F. et al. (2018) Integrated geophysical survey in a sinkhole-prone area: microgravity, electrical resistivity tomographies, and seismic noise measurements to delimit its extension. *Engineering Geology*, 243, 282–293 https://doi.org/10.1016/j.enggeo.2018.07.016

Pearson, M. (2013) *Sinkholes: common, costly and sometimes deadly*. CNN. Retrieved March 7, 2022, from https://edition.cnn.com/2013/03/01/us/florida-sinkhole-explainer/index.html.

Rodriguez, V., Gutiérrez, F., Green, A.G., Carbonel, D., Horstmeyer, H. & Schmelzbach, C. (2014) Characterizing sagging and collapse sinkholes in a mantled karst by means of Ground Penetrating Radar (GPR). *Environmental and Engineering Geosciences*, 20(2), 109–132. https://doi.org/10.2113/gseegeosci.20.2.109

Ronen, A., Ezersky, M., Beck, A., Gatenio, B. & Simhayov, R.B. (2019) Use of GPR method for prediction of sinkholes formation along the Dead Sea Shores, Israel. *Geomorphology*, 328, 28–43. https://doi.org/10.1016/j.geomorph.2018.11.030

Rosso, A. (2022). Si apre una voragine di 20 metri in un terreno a Raveo: inghiottito un frutteto. *Il Piccolo*. Retrieved October 24, 2022, from https://ilpiccolo.gelocal.it/trieste/cronaca/2022/04/22/news/si-apre-una-voragine-di-20-metri-in-un-terreno-a-raveo-inghiottito-un-frutteto-1.41391831

18730604, 2023, 5, Downloaded from https://onlinelibrary.wiley.com/doi/10.1002/nsg.12261 by Universita Di Trieste, Wiley Online Library on [28/01/2025]. See the Terms and Conditions (https://onlinelibrary.wiley.com/terms-and-conditions) on Wiley Online Library for rules of use; OA articles are governed by the applicable Creative Commons License

Saarenketo, T. & Scullion, T. (2000) Road evaluation with ground penetrating radar. *Journal of Applied Geophysics*, 43(2–4), 119–138. https://doi.org/10.1016/S0926-9851(99)00052-X

Samyn, K., Mathieu, F., Bitri, A., Nachbaur, A. & Closset, L. (2014) Integrated geophysical approach in assessing karst presence and sinkhole susceptibility along flood protection dykes of the Loire River, Orléans, France. *Engineering Geology*, 183, 170–184. https://doi.org/10.1016/j.enggeo.2014.10.013

Sevil, J., Gutiérrez, F., Zarroca, M., Desir, G., Carbonel, D., Guerrero, J. et al. (2017) Sinkhole investigation in an urban area by trenching in combination with GPR, ERT and high-precision leveling. Mantled evaporite karst of Zaragoza city, NE Spain. *Engineering Geology*, 231, 9–20. https://doi.org/10.1016/j.enggeo.2017.10.009

Sevil, J., Gutiérrez, F., Carmicer, C., Carbonel, D., Desir, G., Garcià-Arnay, Á. et al. (2020) Characterizing and monitoring a high-risk sinkhole in an urban area underlain by salt through non-invasive methods: detailed mapping, high-precision leveling and GPR. *Engineering Geology*, 272, 105641. https://doi.org/10.1016/j.enggeo.2020.105641

Shi, Y., Tang, Y., Lu, Z., Kim, J.W. & Peng, J. (2019) Subsidence of sinkholes in Wink, Texas from 2007 to 2011 detected by time-series InSAR analysis. *Geomatics, Natural Hazards and Risk*, 10, 1125–1138. https://doi.org/10.1080/19475705.2019.1566786

Solari, L., Montalti, R., Barra, A., Monserrat, O., Bianchini, S. & Crosetto, M. (2020) Multi-temporal satellite interferometry for fast-motion detection: an application to salt solution mining. *Remote Sensing*, 12, 3919. https://doi.org/10.3390/rs12233919

Stierman, D.J. (2004). Geophysical detection of caves and Karstic voids. In: Gunn, J. (Ed.) *Encyclopedia of caves and karst science*. New York: Fitzroy Dearborn, pp. 377–380.

Taheri, K., Gutiérrez, F., Mohseni, H., Raeisi, E. & Taheri, M. (2015) Sinkhole susceptibility mapping using the analytical hierarchy process (AHP) and magnitude–frequency relationships: a case study in Hamadan province, Iran. *Geomorphology*, 234, 64–79. https://doi.org/10.1016/j.geomorph.2015.01.005

Taheri, K., Shahabi, H., Chapi, K., Shirzadi, A., Gutiérrez, F. & Khosravi, K. (2019) Sinkhole susceptibility mapping: a comparison between Bayes-based machine learning algorithms. *Land Degradation and Development*, 30(7), 730–745. https://doi.org/10.1002/ldr.3255

Taheri, K., Missimer, T.M., Mohseni, H., Fidelibus, M.D., Fathollahy, M. & Taheri, M. (2021) Enhancing spatial prediction of sinkhole susceptibility by mixed waters geochemistry evaluation: application of ROC and GIS. *Environmental Earth Sciences*, 80(14), 1–28. https://doi.org/10.1007/s12665-021-09763-8

Talib, O.C., Shimon, W., Sarah, K. & Tonian, R. (2022) Detection of sinkhole activity in West-Central Florida using InSAR time series observations. *Remote Sensing of Environment*, 269, 112793. https://doi.org/10.1016/j.rse.2021.112793

Theron, A., Engelbrecht, J., Kemp, J., Kleynhans, W. & Turnbull, T. (2017) Detection of sinkhole precursors through SAR interferometry: radar and geological considerations. *IEEE Geoscience and Remote Sensing Letters*, 14(6), 871–875. https://doi.org/10.1109/LGRS.2017.2684905

Thierry, P., Prunier-Leparmentier, A.M., Lembezat, C., Vanoudheusden, E. & Vernoux, J.F. (2009) 3D geological modelling at urban scale and mapping of ground movement susceptibility from gypsum dissolution: the Paris example (France). *Engineering Geology*, 105, 51–64. https://doi.org/10.1016/j.enggeo.2008.12.010

Thitimakorn, T., Kampananon, N., Jongjaiwanichkit, N. & Kupongsak, S. (2016) Subsurface void detection under the road surface using ground penetrating radar (GPR), a case study in the Bangkok metropolitan area, Thailand. *International Journal of Geo-Engineering*, 7(2). https://doi.org/10.1186/s40703-016-0017-8

Vennari, C. & Parise, M. (2022) A chronological database about natural and anthropogenic Sinkholes in Italy. *Geosciences*, 12, 200. https://doi.org/10.3390/geosciences12050200

Venturini, C., Spalletta, C., Vai, G.B., Pondrelli, M., Delzotto, S., Fontana, C. et al. (2009) *Note Illustrative Carta geologica d'Italia alla scala 1:50.000 Foglio 031 Ampezzo*. Rome, Italy: ISPRA, pp. 7–222.

Waltham, T., Bell, F. & Culshaw, M. (2005) *Sinkholes and subsidence: karst and cavernous rocks in engineering and construction*. Chichester, UK: Springer. https://doi.org/10.1007/b138363

Wang, Y., Tran, K.T. & Horhota, D. (2022) *Road sinkhole imaging with ambient noise tomography*. Charlotte, North Carolina: Geo-Congress: Geophysical and Earthquake Engineering and Soil Dynamics. https://doi.org/10.1061/9780784484043.004

Wust-Bloch, G.H. & Joswig, M. (2006) Pre-collapse identification of sinkholes in unconsolidated media at Dead Sea area by 'nano-seismic monitoring' (graphical jackknife location of weak sources by few, low-SNR records). *Geophysical Journal International*, 167, 3, 1220–1232, https://doi.org/10.1111/j.1365-246X.2006.03083.x

Yordkayhun, S., Wattanasen, K. & Thungpru, N. (2022) Geophysical investigation of the karst geosites in Satun UNESCO Global Geopark, Thailand: implication for sinkhole hazard assessment. *Geosciences Journal*, 26(2), 249–266. https://doi.org/10.1007/s12303-021-0025-3

Youssef, A.M., El-Kaliouby, H. & Zabramawi, Y.A. (2012) Sinkhole detection using electrical resistivity tomography in Saudi Arabia. *Journal of Geophysics and Engineering*, 9, 655–663. https://doi.org/10.1088/1742-2132/9/6/655

Zhao, W., Forte, E. & Pipan, M. (2016) Texture attribute analysis of GPR data for archaeological prospection. *Pure and Applied Geophysics*, 173, 2237–2251. https://doi.org/10.1007/s00024-016-1355-3

Zhu, J., Taylor, T.P., Currens, J.C. & Crawford, M.M. (2014) Improved karst sinkhole mapping in Kentucky using LiDAR techniques: a pilot study in Floyds Fork watershed. *Journal of Cave and Karst Studies*, 76, 207–216. https://doi.org/10.4311/2013ES0135

Zhu, J., Nolte, A.M., Jacobs, N. & Ye, M. (2020) Using machine learning to identify karst sinkholes from LiDAR-derived topographic depressions in the Bluegrass Region of Kentucky. *Journal of Hydrology*, 588, 125049. https://doi.org/10.1016/j.jhydrol.2020.125049

Zhende, G., Xiaozhen, J., Ming, G. (2013) A calibration test of karst collapse monitor-ing device by optical time domain reflectomewtry (BOTDR) technique. In L. Land, D.H. Doctor, J.B. Stephenson (Eds.), Sinkholes and the engineering and environmental impacts of karst (pp 71.77). Carlsbad, NM: National Cave and Karst Research Institute.

Zini, L., Calligaris, C., Forte, E., Petronio, L., Zavagno, E., Boccali, C. et al. (2015) A multidisciplinary approach in sinkhole analysis: the Quinis village case study (NE-Italy). *Engineering Geology*, 197, 132–144. https://doi.org/10.1016/j.enggeo.2015.07.004

How to cite this article: Calligaris, C., Forte, E., Busetti, A. & Zini, L. (2023) A joint geophysical approach to tune an integrated sinkhole monitoring method in evaporitic environments. *Near Surface Geophysics*, 21, 317–332. https://doi.org/10.1002/nsg.12261

18730604, 2023, 5, Downloaded from https://onlinelibrary.wiley.com/doi/10.1002/nsg.12261 by Universita Di Trieste, Wiley Online Library on [28/01/2025]. See the Terms and Conditions (https://onlinelibrary.wiley.com/terms-and-conditions) on Wiley Online Library for rules of use; OA articles are governed by the applicable Creative Commons License